# Hard Photoproduction and the Structure of the Photon

Laurel Sinclair for the ZEUS and H1 Collaborations

Department of Physics and Astronomy, University of Glasgow, G12 8QQ, UK

**Abstract.** A pedagogical introduction to the experimental results on hard photoproduction at HERA is provided. Then the latest results in this field from ZEUS and H1 are reviewed.

## 1 Introduction

It has now been firmly established that the photon can interact strongly, as though it were a hadron. Indeed, two of the first physics results to be published by the HERA experiments H1 and ZEUS were the measurements of the total photoproduction cross section [1,2]. These confirmed the cross section of the photon to be of order 100 nb, close to the area of a typical hadron.

Of course the total cross section is dominated by peripheral collisions which cannot be described in perturbative QCD. In the presence of a hard scale the photon proton cross section factorizes into terms describing the photon and proton structures, and a hard QCD subprocess. Then a perturbative expansion may be applied to determine the subprocess cross section (for an introduction to the theory of hard photoproduction see Michael Klasen's contribution to this proceedings).

With subsequent data sets H1 and ZEUS measured the photoproduction cross section for events in the perturbatively calculable regime, i.e. with jets of at least $E_T^{\rm jet} > 5$ GeV [3,4]. This cross section is naturally much smaller, of the order of 10 nb, however the hadronic nature of the photon is still prevalent. The HERA experiments clearly established two classes of contribution to the photoproduction of jets: the direct process in which the photon itself participates in the hard subprocess and the resolved process in which the photon fluctuates into a hadronic object and one of its partonic constituents participates in the hard subprocess. For instance, H1 found an excess of energy in the rear direction, over what was expected for direct photoproduction processes [5]. This energy could be attributed to the presence of a photon remnant jet in the resolved photon process.

An unambiguous distinction between resolved and direct processes exists only at leading order (LO). In Figures 1(a) and (b) examples of direct diagrams in LO and next-to-leading order (NLO), respectively, are shown. Figure 1(c) shows an example of a resolved diagram at leading order. Clearly, if the outgoing quark line in the NLO direct diagram 1(b) has small transverse momentum then this process could as well be represented by the LO resolved diagram 1(c). Therefore

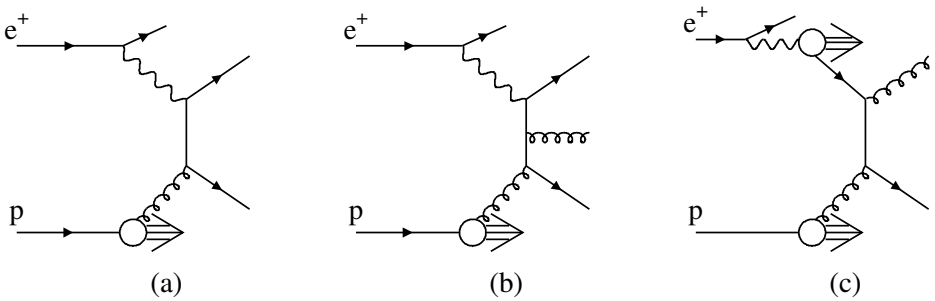


**Fig. 1.** Illustration of diagrams for (**a**) LO direct (**b**) NLO direct and (**c**) LO resolved photoproduction processes

some prescription must be introduced in order to make a well-defined distinction between direct and resolved processes.

To this end the observable quantity $x_\gamma^{\rm OBS}$ has been defined:

$$x_\gamma^{\rm OBS} \equiv \frac{\sum_{\rm jets} E_T^{\rm jet} e^{-\eta^{\rm jet}}}{2yE_e},$$

where $E_T^{\rm jet}$ and $\eta^{\rm jet}$ are the jet transverse energy and pseudorapidity respectively, $y$ is the fraction of the electron's energy carried by the incoming photon, $E_e$ is the incoming electron energy, and the sum runs over the two highest $E_T^{\rm jet}$ jets within the $\eta^{\rm jet}$ acceptance. At leading order $x_\gamma^{\rm OBS} = 1$ for direct processes and $x_\gamma^{\rm OBS} < 1$ for resolved processes. However, $x_\gamma^{\rm OBS}$ is well defined theoretically to any order of perturbation theory (provided, of course, that the jet-finding algorithm is well-behaved). Therefore, a quantitative confrontation of a measurement of a "direct" or "resolved" photoproduction cross section with a pQCD calculation can be made provided the separation between the direct and resolved regions is made in terms of $x_\gamma^{\rm OBS}$.

In Figure 2 a measured $x_\gamma^{\rm OBS}$ distribution is shown for photoproduction events containing two jets of $E_T^{\rm jet1,\ jet2} > 11, 14$ GeV within $-1 < \eta^{\rm jet} < 2$ in the HERA lab frame [6]. The data show a peak at high $x_\gamma^{\rm OBS}$ values with a broad tail extending to $x_\gamma^{\rm OBS} \sim 0$. The data are compared with the predictions of two parton shower Monte Carlo programs, HERWIG 5.9 [7,8] and PYTHIA 5.7 [9,10]. The Monte Carlo calculations implement the QCD matrix elements at leading order only. The effect of higher order processes is approximated through initial and final-state parton showers. The programs differ in the choice of evolution variable for the parton shower calculation and also in the technique chosen to convert the final partonic configuration into colourless hadrons. Both are able to provide a good description of the $x_\gamma^{\rm OBS}$ distribution. The distribution of the HERWIG events with LO direct photoproduction subprocesses is shown separately as the shaded histogram. The parton showering and hadronizaton

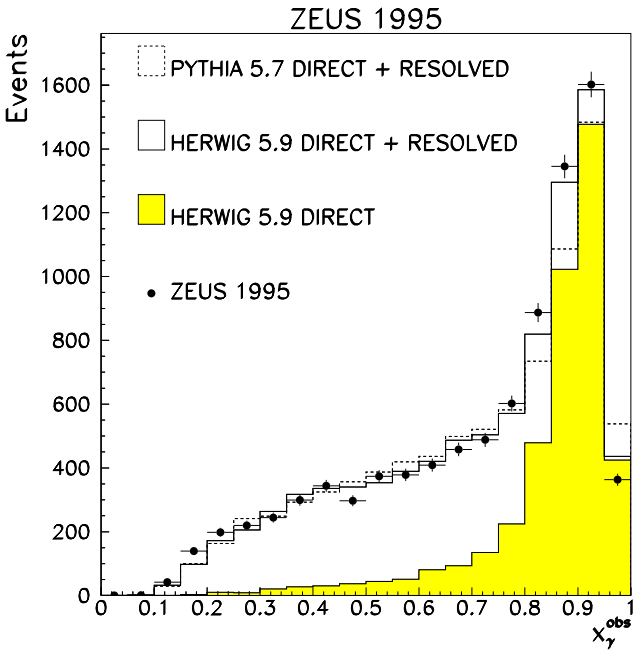


**Fig. 2.** The $x_\gamma^{\mathrm{OBS}}$ spectrum for events with $E_T^{\mathrm{jet1,\ jet2}} > 11, 14$ GeV, compared to the HERWIG 5.9 and the PYTHIA 5.7 Monte Carlo predictions. The direct component from the HERWIG Monte Carlo is shown separately as the shaded histogram. Only statistical uncertainties are plotted

phases smear the $x_\gamma^{\mathrm{OBS}}$ values such that this distribution is peaked just below one and can extend to the lowest available $x_\gamma^{\mathrm{OBS}}$ values. Nevertheless it is plain to see that a sample of events with $x_\gamma^{\mathrm{OBS}} > 0.75$ is essentially of the direct photoproduction type. ZEUS and H1 have published several papers in which direct and resolved photoproduction regions are defined based on the $x_\gamma^{\mathrm{OBS}}$ observable [4,6,11–19]

An important confirmation of the presence of the direct and resolved contributions to photoproduction was provided by the ZEUS measurement of dijet scattering angles [13]. A two jet final state can be completely specified in its centre-of-mass frame (up to an arbitrary azimuthal rotation) by the dijet invariant mass, $M_{2\mathrm{J}}$, and the dijet scattering angle, $\vartheta^*$. Direct photoproduction processes should proceed predominantly through quark exchange (the diagram shown at leading order in Figure 1(a)). As the exchanged parton is of spin 1/2, at leading order the dijet scattering angle is distributed according to $1/(1-|\cos\vartheta^*|)$. In contrast, resolved processes are dominated by the exchange of the integer spin gluon which gives rise to the steeper angular dependence, $1/(1-|\cos\vartheta^*|)^2$. ZEUS observed a steeper angular dependence for the events with $x_\gamma^{\mathrm{OBS}} < 0.75$ than for those with $x_\gamma^{\mathrm{OBS}} \geq 0.75$, as shown in Figure 3.

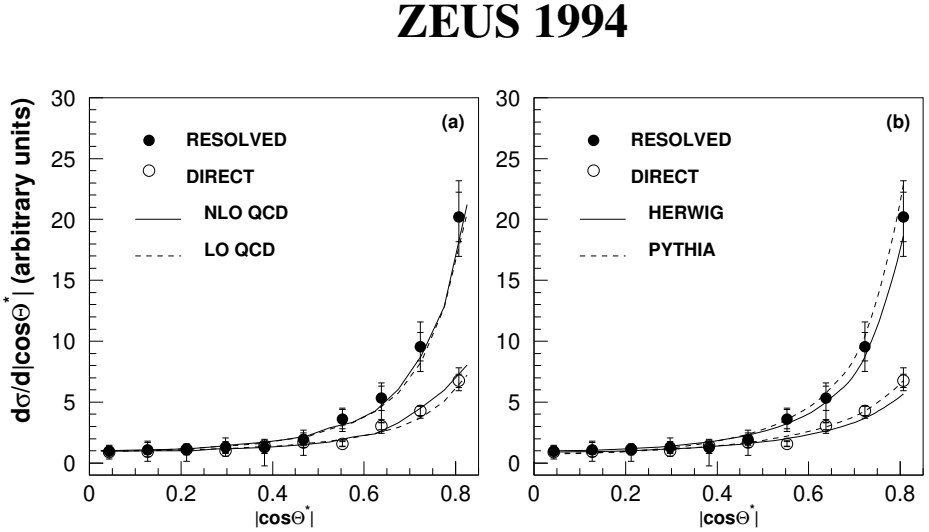


**Fig. 3.** $d\sigma/d|\cos\vartheta^*|$ normalized to one at $\cos\vartheta^* = 0$ for $x_\gamma^{\rm OBS} < 0.75$ (*black dots*) and $x_\gamma^{\rm OBS} \geq 0.75$ (*open circles*) photoproduction. In (**a**), the ZEUS data are compared to NLO predictions (*solid line*) and LO predictions (*broken line*). In (**b**), the broken line is the PYTHIA distribution and solid line is the HERWIG distribution. The inner error bars are the statistical errors, the outer error bars are the sum in quadrature of the statistical and systematic uncertainties

This is a compelling observation. An invariant mass cut of $M_{2\rm J} > 23$ GeV has been applied to ensure that the $E_T^{\rm jet} > 6$ GeV requirement does not bias the angular distribution. Moreover, the dijet scattering angle is defined in the centre-of-mass frame of the two jets so the fact that the lower $x_\gamma^{\rm OBS}$ events are boosted more in the proton direction is not responsible for the differences observed in the $\cos\vartheta^*$ distributions. The different $\cos\vartheta^*$ distributions for the high and low $x_\gamma^{\rm OBS}$ samples are therefore an unambiguous demonstration of the differing underlying QCD subprocess dynamics. There is a greater contribution from gluon exchange processes contributing to the $x_\gamma^{\rm OBS} < 0.75$ sample, than there is contributing to the $x_\gamma^{\rm OBS} \geq 0.75$ sample. This is consistent with the expectation that more resolved photon processes contribute to the $x_\gamma^{\rm OBS} < 0.75$ sample.

Thus it has been established that both direct and resolved processes contribute to photoproduction at HERA. The study of these processes is now providing a fruitful forum for the investigation of strong interactions. Photoproduction processes access the physics involved in the structures of the photon and proton, in the dynamics of hard subprocesses, and in the fragmentation and hadronization of the final state partons.

The structure of the photon is probed in deep inelastic $e\gamma$ experiments at $e^+e^-$ colliders in just the same way as the structure of the proton is probed in $ep$

interactions at HERA. These measurements of the photon's structure function, $F_2^\gamma$, constrain the quark densities at intermediate probing energy scales. However, the gluon density is not directly constrained in these experiments, nor do the quark density constraints extend to the high energy scale region accessible at HERA. It is in these two areas that the HERA experiments have concentrated their efforts.

Phenomenological ansätze for the parton densities of the photon exist. These generally involve the assumption that at low probing virtualities, the photon undergoes a quantum fluctuation into a vector meson or an unbound $q\bar{q}$ state and this provides the photon's structure. A DGLAP evolution is then invoked in order to evolve the parton densities to arbitrary scale, using the $e\gamma$ $F_2^\gamma$ data as a constraint. Thus, studies of photoproduction sensitive to the photon's structure test fundamental physical assumptions, in addition to providing a means to investigate the universality of photon structure data obtained through different processes. In sections 2 and 3 the latest results from H1 and ZEUS pertaining to the structure of the photon are presented.

Perturbative QCD governs the behaviour of the partons emerging from the hard subprocess. As the distribution of the jets of hadrons in the final state bears a close correspondence to the distribution of the underlying partons, measurements may be designed which are sensitive to the subprocess dynamics. The differing dijet angular distributions for direct and resolved photoproduction have already been discussed. As the available luminosity delivered by HERA has increased, it has become possible to look for unusual dynamical signatures in high $E_T^{\rm jet}$ dijet processes, and also to investigate the underlying mechanism of three jet production. Studies of the matrix element dynamics are presented in section 4.

Our knowledge is limited about the physics of hadronization, whereby the partons resulting from a collision are converted to colourless hadrons by the inexorable confinement force of QCD. The hadronization occurs at low momentum transfers where the QCD coupling is much too strong for a perturbative expansion to be relevant. However, there are experimental results which have provided some information about this interesting area of physics. For instance, a universality of the hadronization of quarks is supported by the measurements of jet shapes in $ep$ and $e^+e^-$ collisions [20]. Recently, a procedure for measuring jet structure in hadronic collisions has been proposed which is valid for an all-orders calculation in perturbative QCD [21]. In this way, a well-defined comparison of theory and data can be undertaken which begins well within the regime where a perturbative approach should be valid and then approaches the mysterious realm of the very strong hadron producing force. A measurement of jet substructure using this algorithm is presented in Section 5.

## 2 Real Photon Structure

A measurement which is sensitive to the gluon density of the photon has been made by the H1 collaboration [22]. The gluonic component of the photon dom-

inates at low $x_\gamma$. Therefore the events must be selected keeping $E_T^{\rm jet}$ as low as possible and allowing $\eta^{\rm jet}$ to extend as far forward into the incoming proton direction as possible. This is a difficult kinematic region experimentally, as the energy-scale uncertainty and angular resolution of the calorimeter are worst here. There are also theoretical limitations as the contribution from events in which there is a secondary scatter, and the smearing between a partonic and hadronic distribution, increase as $E_T^{\rm jet}$ lowers. Nevertheless it has been possible to make the measurement with sufficient precision to illustrate the sensitivity of the data to the distribution of gluons in the photon. Figure 4 shows $d\sigma/dx_\gamma^{\rm jets}$ [1] for events containing two jets of $E_T^{\rm jet} > 6$ GeV within $-0.5 < \eta^{\rm jet} < 2.5$. The data are compared with the predictions of the leading order plus parton shower Monte Carlo program PHOJET [23,24] where the predictions including and neglecting the gluons in the photon are shown separately. Although there is a large systematic uncertainty affecting the measurement, within the PHOJET model

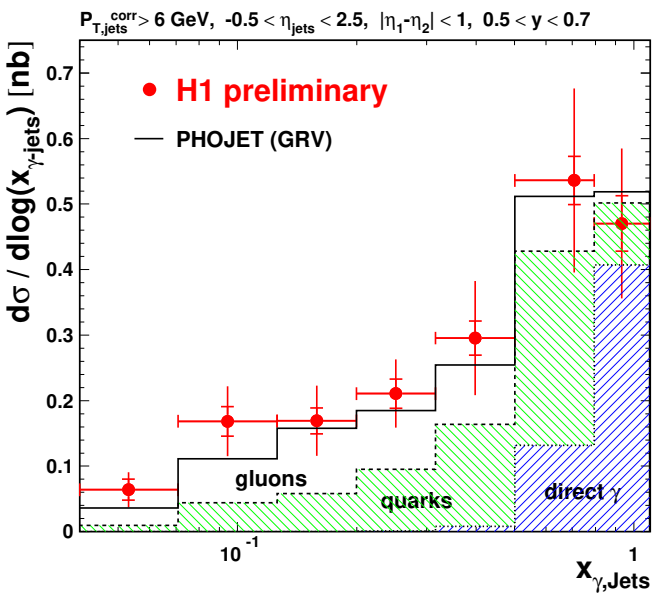


**Fig. 4.** Dijet cross section in photproduction as a function of $x_\gamma^{\rm jets}$. The data are compared to the prediction of PHOJET. The direct photon prediction, and the resolved photon predictions for either quarks are gluons, are shown separately

a significant gluonic contribution at low $x_\gamma^{\rm jets}$ is required by the data assuming the GRV-LO [25,26] parton densities for the photon and proton.

H1 have gone on to subtract the influence of secondary parton scattering and unfold the data to a leading order effective parton density, using the Monte

[1] $x_\gamma^{\rm jets}$ is essentially the same quantity as has been called $x_\gamma^{\rm OBS}$.

Carlo model. From this the modelled quark density has been subtracted to yield the gluon density as a function of $x_\gamma$ where now $x_\gamma$ refers to the fraction of the momentum of the photon which enters the leading order hard subprocess. This is necessarily a model dependent result; however it can serve to provide insight into photon structure. H1 finds that the gluon density rises as $x_\gamma$ decreases.

The ZEUS analysis of photon structure has concentrated on limiting the data to that kinematic regime in which perturbative QCD should be applicable, without the need for additional model parameters. Dijet events have been selected with $E_T^{\mathrm{jet1,\ jet2}} > 11,14$ GeV within $-1 < \eta^{\mathrm{jet}} < 2$ [6]. The $x_\gamma^{\mathrm{OBS}}$ distribution for this selection is shown in Figure 2. The PYTHIA and HERWIG predictions which are compared with the data in this figure contain no simulation of soft underlying events or of secondary parton scatterings and provide a good description of the data. Also, studies have indicated that hadronization effects in this kinematic regime should be small, at most around 10%. Therefore a strong interpretation of this data within perturbative QCD can be made.

In Figure 5 the cross section for the $E_T^{\mathrm{jet1,\ jet2}} > 11,14$ GeV selection, $d\sigma/d\eta_1^{\mathrm{jet}}$, is shown in bins of $\eta_2^{\mathrm{jet}}$. The kinematic region is restricted to a narrow $y$ range, in order to improve the sensitivity to the photon's structure. The cross section is shown separately for $x_\gamma^{\mathrm{OBS}} \geq 0.75$, indicating that the direct process dominates when the jets tend toward the incoming photon direction. NLO perturbative QCD predictions with the three available photon parton parametrizations [25,27–29] are compared with the data in this figure. (Note that the calculations have been checked by several different groups of theorists as reported in [30].) The predictions underestimate the data in the central rapidity region where experimental and theoretical uncertainties are expected to be particularly small. As previously mentioned, the parton density of the photon is not well constrained by $e\gamma$ data at these high energy scales. Therefore it is expected that the parton density of the photon may be underestimated in this kinematic regime in the currently available parton density functions of the photon.

In another interesting analysis by H1 the photon remnant jet has been tagged in low $x_\gamma^{\mathrm{jet}}$ events by running a clustering algorithm, requiring exactly four jets in the event and defining the photon remnant jet as that jet closest to the incoming photon direction [31]. The $E_T^{\mathrm{jet}}$ of the remnant jet was found to be correlated with the $E_T^{\mathrm{jet}}$ of the highest transverse energy jets. This points to the presence of the anomalous component of the photon's structure whereby the struck parton arises from a $q\bar{q}$ splitting of the photon rather than as a constituent of a fluctuation into a vector meson. The "remnant jet" can then, as in Figure 1(b), be viewed instead as one of the outgoing partons from a next-to-leading order hard subprocess.

Another promising process for constraining the parton density of the photon is prompt photon production, in which an outgoing quark from the hard subprocess is balanced not by a gluon, but by a photon (see [30] for a complete discussion of the contributing diagrams). ZEUS has published a measurement of the cross section for prompt photon production in association with a jet [32]. A more inclusive measurement, whereby only the prompt photon is tagged without the jet

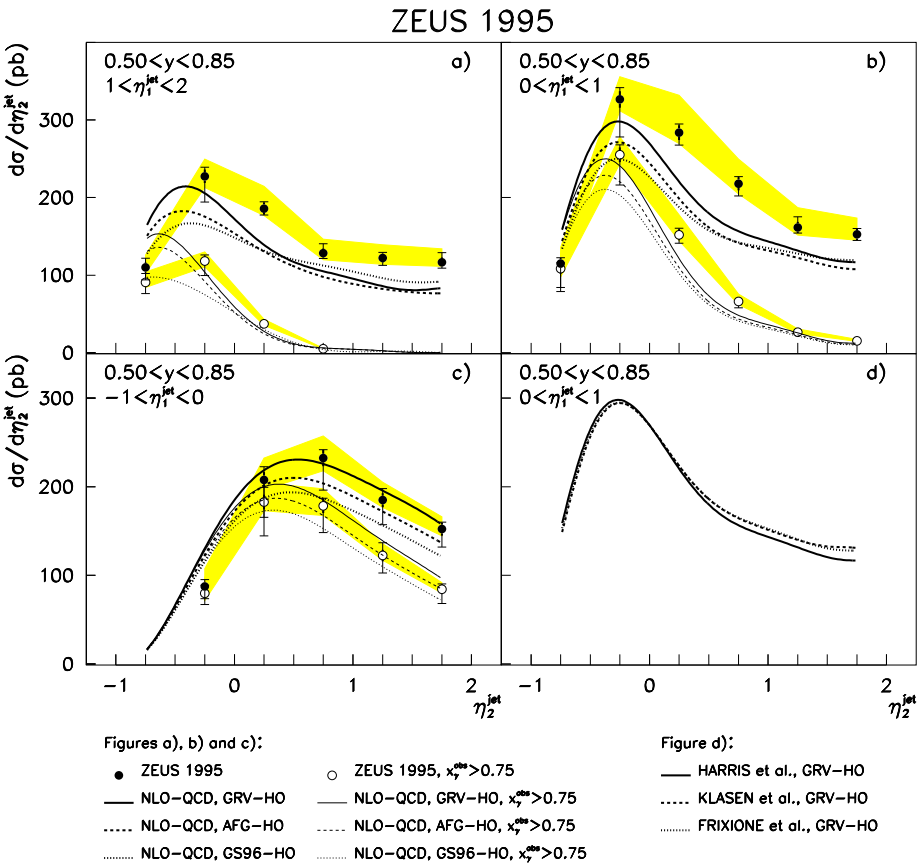


**Fig. 5.** Figures (**a**), (**b**) and (**c**) show the dijet cross section as a function of $\eta_2^{\rm jet}$ in bins of $\eta_1^{jet}$. The filled circles correspond to the entire $x_\gamma^{\rm OBS}$ range while the open circles correspond to events with $x_\gamma^{\rm OBS} > 0.75$. The shaded band indicates the uncertainty related to the energy scale. The thick error bar indicates the statistical uncertainty and the thin error bar indicates the systematic and statistical uncertainties added in quadrature. The full, dotted and dashed curves correspond to NLO-QCD calculations, using the GRV-HO, GS96-HO and the AFG-HO parameterizations for the photon structure, respectively. In (**d**) the NLO-QCD results for the cross section when $0 < \eta_1^{\rm jet} < 1$ and for a particular parameterization of the photon structure are compared

requirement, is free of complications due to the matching of the jet definition in theory and experiment and relatively free of hadronization corrections. This then, like high $E_T^{\rm jet}$ production, is an area in which a strong interpretation can be made from the comparision of the data with the predictions of perturbative QCD. Of course the cross section for prompt photon production is suppressed

with respect to jet production due to the smallness of the electromagnetic coupling constant and currently the statistics are limited. Nevertheless the technique of prompt photon identification has been refined and a first comparison with the theory indicates a rough agreement [30].

## 3 Virtual Photon Structure

It is expected that as the virtuality of the incoming photon increases, less time will be available for it to develop a complex hadronic structure. To test this assumption, H1 has measured the dijet triple differential cross section, $d\sigma_{ep}/(dQ^2 d\bar{E_t}^2 dx_\gamma^{\rm jets})$ where $\bar{E_t}$ is the average jet transverse energy and $Q^2$ is the negative of the square of the momentum transfer at the scattered lepton vertex [14]. The cross section is presented in Figure 6 as a function of $x_\gamma^{\rm jets}$ in bins of $\bar{E_t}^2$ in the range $30 < \bar{E_t}^2 < 300$ GeV$^2$ and in bins of $Q^2$ in the range $1.6 < Q^2 < 25$ GeV$^2$. The data are concentrated near $x_\gamma^{\rm jets} = 1$ with a small tail to lower values. Compared with the data are predictions from the HERWIG model, where the events with a leading order direct subprocess are shown separately by the shaded histogram. Looking at fixed $\bar{E_t}^2$, there is clear evidence for the expected suppression of the resolved processes as $Q^2$ increases. However, wherever $\bar{E_t}^2 \gg Q^2$, the direct processes alone are insufficient to account for the low $x_\gamma^{\rm jets}$ events. Thus there is evidence for resolved photon processes, even well into the deep inelastic scattering regime, $Q^2 > 8$ GeV$^2$.

H1 have extended the analysis in their publication [14] and unfolded the data to a leading order effective parton density, $f_{\rm eff} \equiv \sum_i^{N_f}(q_i + \bar{q}_i) + \frac{9}{4}g$, relying on the Monte Carlo simulation to correct the data for hadronization and higher order effects. The behaviour of this parton density is consistent with a logarithmic rise with the probing resolution, $P_t^2$, where $P_t$ is the transverse momentum of the two outgoing partons at leading order. This is in contrast with the approximate scaling behaviour which has been observed for hadrons and reflects the presence of the anomalous, or $q\bar{q}$ splitting term, unique to the structure of the photon.

The effective parton density is also found to exhibit a dependence on the photon's virtuality $Q^2$ which is consistent with the expected logarithmic suppression implemented in the existing virtual photon parton density functions. Incorporating an earlier measurement of $f_{\rm eff}$ at $Q^2 = 0$ with these data, a drop in $f_{\rm eff}$ with $Q^2$ is indicated. (To compare the earlier measurement with this one the data have been evolved using the GRV LO parton densities to the same $P_t^2$ and $x_\gamma$ range.)

The ZEUS collaboration has measured the dijet cross section $d\sigma/dx_\gamma^{\rm OBS}$ for jets of $E_T^{\rm jet} > 5.5$ GeV in the three different photon virtuality ranges $Q^2 \sim 0$ ($Q^2 < 1$ GeV$^2$), $0.1 < Q^2 < 0.55$ GeV$^2$ and $1.5 < Q^2 < 4.5$ GeV$^2$ [33]. This measurement is complementary to the H1 analysis in that the $Q^2 \sim 0$ data are analyzed together with the deep inelastic data at $1.5 < Q^2 < 4.5$ GeV$^2$ in a consistent way. Also, making use of an auxiliary small angle electron tagger, the

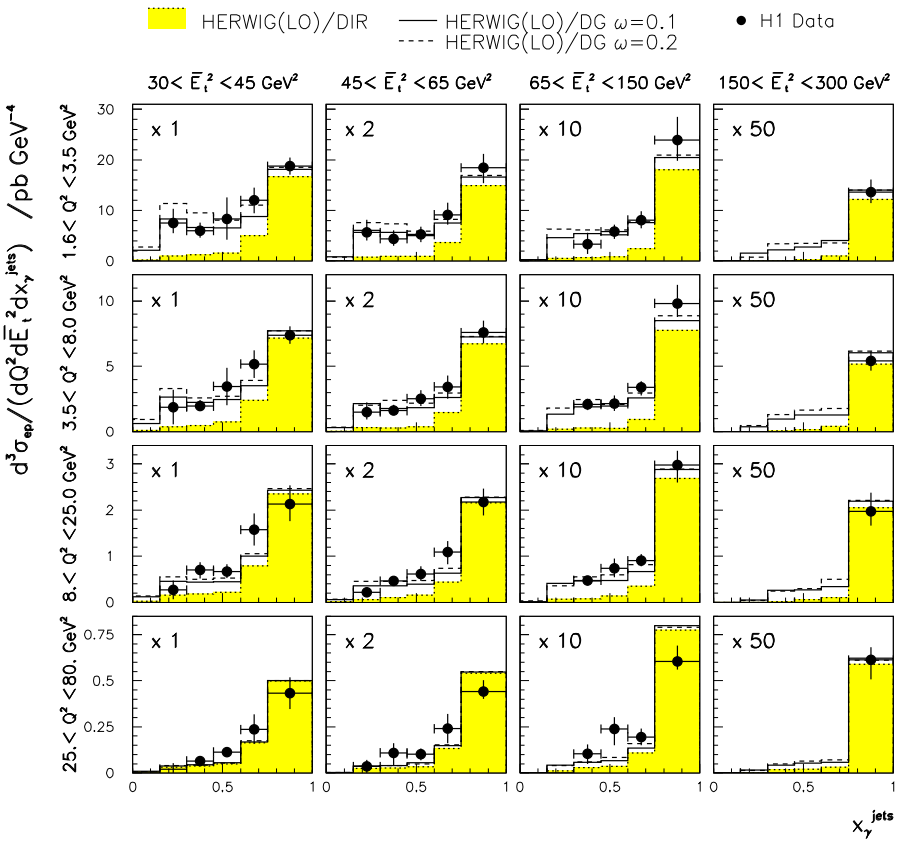


**Fig. 6.** The differential dijet cross section $d\sigma_{ep}/(dQ^2 d\bar{E}_t{}^2 dx_\gamma^{\rm jets})$ shown as a function of $x_\gamma^{\rm jets}$ for different regions of $\bar{E}_t$ and $Q^2$. The scale factors applied to the cross sections are indicated. The error bar shows the quadratic sum of systematic and statistical errors. Also shown is the HERWIG model where the direct component is shown as the shaded histogram

ZEUS measurement includes data in the important transition region between photoproduction and deep inelastic scattering, $0.1 < Q^2 < 0.55$ GeV$^2$. From the $d\sigma/dx_\gamma^{\rm OBS}$ measurements, similar conclusions can be drawn as in the H1 analysis: the population of the $x_\gamma^{\rm OBS}$ distribution is suppressed at low values as $Q^2$ increases yet there is evidence for a resolved component of the photon even in the deep inelastic scattering regime, $Q^2 > 1.5$ GeV$^2$.

In order to make a precise statement concerning the evolution of the virtual photon parton densities with $Q^2$, ZEUS has measured the ratio of the dijet cross section for $x_\gamma^{\rm OBS} < 0.75$ to that for $x_\gamma^{\rm OBS} \geq 0.75$ in bins of $Q^2$ [33]. The result

is shown in Figure 7. The ratio of resolved to direct cross sections is found to fall with $Q^2$. In comparison, this ratio within the HERWIG model is flat for a

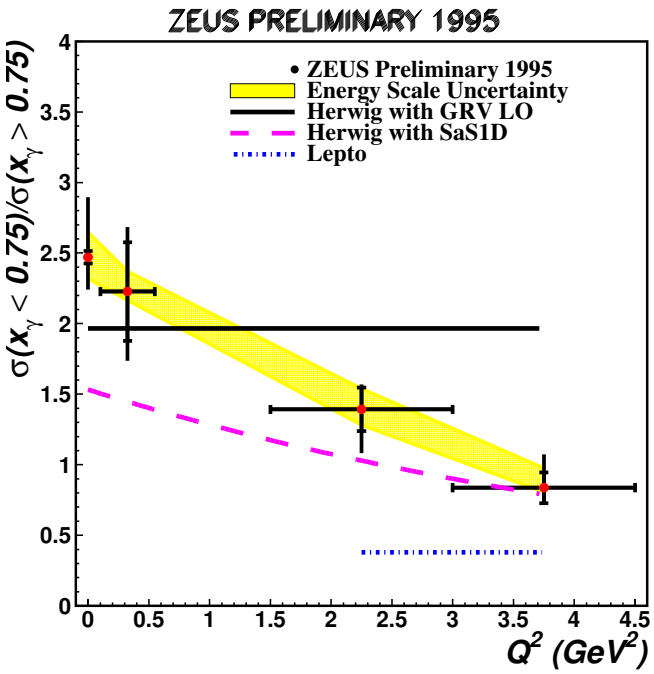


**Fig. 7.** The ratio of dijet cross sections, $\sigma(x_\gamma^{\rm OBS} < 0.75)/\sigma(x_\gamma^{\rm OBS}) \geq 0.75)$, as a function of photon virtuality, $Q^2$. The inner error bar represents the statistical error and the outer the statistical and systematic uncertainties added in quadrature. The band represents the systematic uncertainty due to the jet energy scale. Also shown are the predictions of HERWIG for two different choices for photon parton densities: GRV for real photons (*full line*) and SaS 1D (*dashed line*) which includes a suppression of the photon parton density with increasing photon virtuality. The LEPTO predictions are shown for $Q^2 > 1.5$ GeV$^2$ (*dot-dashed line*)

photon parton density which does not fall with $Q^2$ (GRV LO) and falling for a photon parton density which does (SaS 1D [34]). Therefore the data indicate that the photon parton density is suppressed with $Q^2$ in this LO description. Furthermore, as $Q^2$ increases the data tend toward a leading order prediction which does not include any resolved photon contribution (Lepto 6.5.1 [35]).

## 4 QCD Matrix Elements

The influence of the dominant QCD subprocesses on dijet angular distributions for events with $M_{2\rm J} > 23$ GeV has been observed, as already discussed. As the integrated luminosity delivered by HERA continues to increase, it is important

to re-measure these distributions in the newly accessible kinematic regimes, in order to check for new contributing processes to dijet production. Using the 1995 to 1997 integrated data set ZEUS has measured the $M_{2\mathrm{J}}$ and $\cos\vartheta^*$ distributions in the kinematic regime $M_{2\mathrm{J}} > 47\,\mathrm{GeV}$ and $|\cos\vartheta^*| < 0.8$ [36]. The measurement extends to a dijet invariant mass of $M_{2\mathrm{J}} \sim 140$ GeV, and the mass and angular distributions are well described by the predictions of perturbative QCD.

For three massless jets, five quantities are necessary to define the system. These are defined in terms of the energies, $E_i$, and momentum three-vectors, $\boldsymbol{p}_i$, of the jets in the three-jet centre-of-mass frame and $\boldsymbol{p}_B$, the beam direction. They are the three-jet invariant mass, $M_{3\mathrm{J}}$; the energy-sharing quantities $X_3$ and $X_4$, $X_i \equiv 2E_i/M_{3\mathrm{J}}$; the cosine of the scattering angle of the highest energy jet with respect to the beam, $\cos\vartheta_3 \equiv \boldsymbol{p}_B \cdot \boldsymbol{p}_3/(|\boldsymbol{p}_B||\boldsymbol{p}_3|)$; and $\psi_3$, the angle between the plane containing the highest energy jet and the beam and the plane containing the three jets, $\cos\psi_3 \equiv (\boldsymbol{p}_3 \times \boldsymbol{p}_B) \cdot (\boldsymbol{p}_4 \times \boldsymbol{p}_5)/(|\boldsymbol{p}_3 \times \boldsymbol{p}_B||\boldsymbol{p}_4 \times \boldsymbol{p}_5|)$, where the jets are numbered, 3, 4 and 5 in order of decreasing energy. ZEUS has measured the three-jet cross section in the kinematic regime defined by $M_{3\mathrm{J}} > 50$ GeV, $|\cos\vartheta_3| < 0.8$ and $X_3 < 0.95$ [37]. (In fact, the events have been further required to have at least two jets with $E_T^{\mathrm{jet}} > 6$ GeV and a third jet with $E_T^{\mathrm{jet}} > 5$ GeV, however these cuts are largely irrelevant because high $E_T^{\mathrm{jet}}$ values are forced by the energy and angular cuts.) The measured cross section is well described by $\mathcal{O}(\alpha\alpha_s^2)$ perturbative QCD calculations both in normalization and in the shapes of the $M_{3\mathrm{J}}$, $X_i$, $\cos\vartheta_3$ and $\psi_3$ distributions.

The measured angular distributions are of particular interest since they differ markedly from the expectation for three jets distributed evenly over the available phase space, and are therefore sensitive to the underlying physical dynamics. The $\cos\vartheta_3$ distribution, since it is primarily determined by the distribution of the highest energy jet, is similar in three jet production to the distribution of $\cos\vartheta^*$ in two jet production. However, $\psi_3$ is determined by the orientation of the third, or softest, jet. For orientations in which the third jet is radiated close to the plane defined by the highest energy jet and the beam, $\psi_3 \sim 0$ or $\pi$. The data are shown in Figure 8. They indicate that configurations in which the third jet is far from the plane containing the highest energy jet and the beam ($\psi_3 \sim \pi/2$) are suppressed. The dip at $\psi_3 = 0$ and $\pi$ is caused by a loss of phase space at low angles due to the $E_T^{\mathrm{jet}\ 3} > 5$ GeV requirement. Taking this into consideration, the data indicate a strong tendency for the three-jet plane to lie close to the plane containing the highest energy jet and the beam.

To aid in the development of a mental picture for three jet production, the data have been compared to the predictions of the PYTHIA and HERWIG models. The hard subprocess is included only at leading order in these models so three-jet events arise from the parton shower phase of the simulation. Parton showers do a remarkably good job of simulating three-jet production as is evident from the agreement of the models with the data in the $\psi_3$ distribution. Within the PYTHIA model it is possible to switch off the simulation of QCD colour coherence. With no simulation of coherence, PYTHIA predicts a relatively uniform population of the $\psi_3$ distribution, as shown in Figure 8. Colour coherence

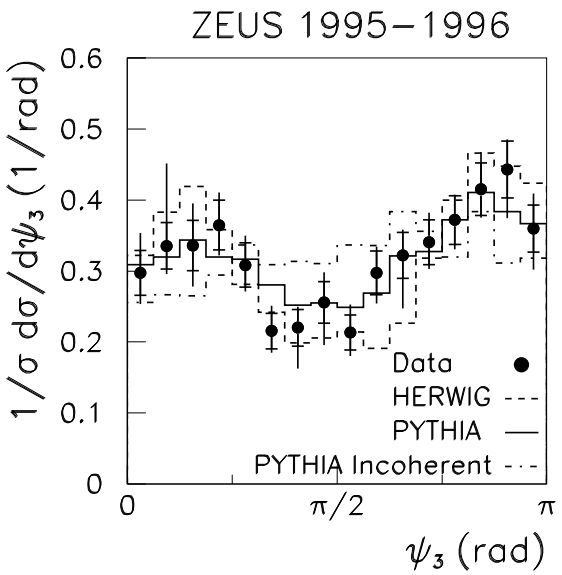


**Fig. 8.** The area-normalized distribution of $\psi_3$. The inner error bar shows the statistical error and the outer error bar shows the quadratic sum of the statistical and systematic uncertainties. The solid histogram shows the default PYTHIA prediction. The dashed and dot-dashed histograms show the predictions of HERWIG and of PYTHIA with colour coherence switched off

in the parton shower model is required to describe the observed suppression of large angle radiation.

## 5 Jet Substructure

The $k_T$ jet-finding algorithm [38,39] clusters objects into jets based on a distance parameter which is essentially their relative transverse momentum. Subjets may be defined within jets by applying the $k_T$ algorithm to the particles of the jet and counting the subjets as a function of the resolution parameter, $y_{\rm cut}$. For large values of $y_{\rm cut}$ there is only one subjet, the jet itself, but as $y_{\rm cut}$ decreases more and more subjets are resolved until the subjet multiplicity equals the multiplicity of particles within the jet.

The dependence of the average number of subjets, $\langle n_{\rm subjet}\rangle$, on $y_{\rm cut}$ has been measured by the ZEUS collaboration for an inclusive sample of jets with $E_T^{\rm jet} > 15$ GeV [40]. Both the HERWIG and PYTHIA models provide a good description of the evolution of $\langle n_{\rm subjet}\rangle$ with $y_{\rm cut}$. Measurements of $\langle n_{\rm subjet}\rangle$ for $y_{\rm cut} = 0.01$ have been performed in four different jet pseudorapidity regions, as presented in Figure 9. The average number of subjets increases as the jets move toward the incoming proton direction. This behaviour is well described by the PYTHIA and HERWIG models. In the models the dominant leading

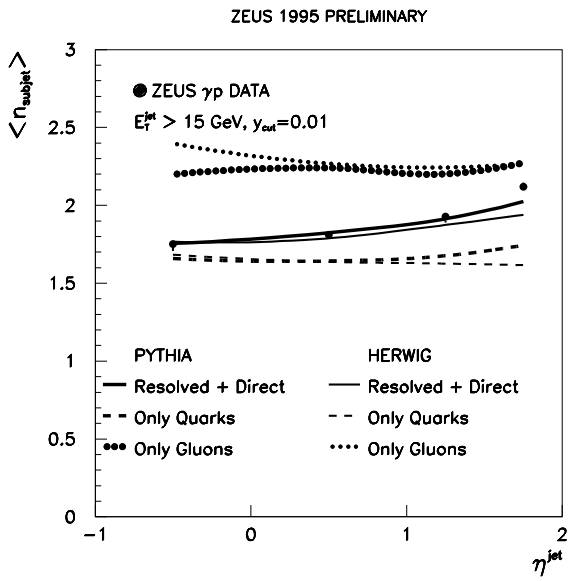


**Fig. 9.** The mean subjet multiplicity at a fixed value of $y_{\rm cut} = 0.01$ as a function of $\eta^{\rm jet}$. The error bars show the statistical and systematic uncertainties added in quadrature. For comparison, the predictions of PYTHIA including resolved plus direct processes for quark jets (*thick dashed line*), gluon jets (*thick dotted line*), and all jets (*thick solid line*) are shown. The predictions of HERWIG are displayed with thin lines

order direct process is $\gamma g \to q\bar{q}$ while the dominant resolved process is $qg \to qg$. Therefore, relatively more gluon jets are expected for the more forward boosted resolved photon processes. Moreover, the gluon in the $qg \to qg$ subprocess has a tendency to be the more forward parton, further increasing the gluonic content of forward jets. The fundamental expectation of QCD that gluons, which have a higher colour charge than quarks, should yield a higher multiplicity of hadrons, is borne out in the models by a higher average subjet multiplicity for gluon jets than for quark jets. Thus the increase of $\langle n_{\rm subjet} \rangle$ with $\eta^{\rm jet}$ may be understood to arise from an increasing admixture of gluon jets in the forward direction. We look forward to an eventual comparison of this data with perturbative QCD calculations.

## 6 Summary

Hard photoproduction events have been used in a variety of analyses in order to further the understanding of the physics of strong interactions. From studies of the structure of the real photon it has been shown that in a leading order interpretation of the data the gluon density rises as the momentum fraction of the photon accessed in the hard subprocess decreases. There is also an indication that the quark densities of the real photon may be underestimated at high momentum

fractions and for high values of the probing energy scale. A global fit of $e\gamma$ and $\gamma p$ measurements should be undertaken to discover whether a parton density can be found which describes all the data. Studies of the structure of the virtual photon have illustrated the expected suppression in the photon's structure as its lifetime decreases. Measurements sensitive to the underlying QCD dynamics have shown that $\mathcal{O}(\alpha\alpha_s^2)$ perturbative QCD matrix elements, and models with $\mathcal{O}(\alpha\alpha_s)$ matrix elements together with parton showers, are successful in explaining the mechanisms of high mass dijet and three-jet production. A measurement of jet substructure has shown the sensitivity of jets produced in hard photoproduction processes to quark and gluon jet differences and revealed their potential to provide insight into the physics of hadronization. Results from photoproduction at HERA have progressed from simple manifestations of the photon's hadronic structure, to detailed investigations of that structure and of QCD in general. As the yearly luminosity deliverable by HERA continues to increase, and as the dialogue between theorists and experimentalists is continuously strengthened, one may look forward to an even greater variety and quality of physics result to emerge from the investigation of hard photoproduction at HERA.

## References


1. ZEUS Collaboration, M. Derrick et al.: Phys. Lett. B **293**, 465 (1992)
2. H1 Collaboration, T. Ahmed et al.: Phys. Lett. B **314**, 436 (1993)
3. H1 Collaboration, I. Abt et al.: Phys. Lett. B **322**, 287 (1994)
4. ZEUS Collaboration, M. Derrick et al.: Phys. Lett. B **322**, 287 (1994)
5. H1 Collaboration, T. Ahmed et al.: Phys. Lett. B **297**, 205 (1993)
6. ZEUS Collaboration, J. Breitweg et al.: *DESY 99-057*
7. G. Marchesini et al., Comp. Phys. Commun. **67**, 465 (1992)
8. G. Marchesini et al., hep-hp/9607393
9. H.U. Bengtsson and T. Sjöstrand, Comp. Phys. Commun. **46**, 43 (1987)
10. T. Sjöstrand, Comp. Phys. Commun. **82**, 74 (1994)
11. ZEUS Collaboration, M. Derrick et al.: Phys. Lett. B **348**, 665 (1995)
12. H1 Collaboration, T. Ahmed et al.: Nucl. Phys. B **445**, 195 (1995)
13. ZEUS Collaboration, M. Derrick et al.: Phys. Lett. B **384**, 401 (1996)
14. H1 Collaboration, C. Adloff et al.: *DESY 98-205*
15. H1 Collaboration, C. Adloff et al.: Eur. Phys. J. **C1**, 97 (1998)
16. ZEUS Collaboration, J. Breitweg et al.: Eur. Phys. J. **C1**, 109 (1998)
17. ZEUS Collaboration, J. Breitweg et al.: Eur. Phys. J. **C5**, 41 (1998)
18. H1 Collaboration, C. Adloff et al.: *DESY 98-148* to appear in Eur. Phys. J. C
19. ZEUS Collaboration, J. Breitweg et al.: Eur. Phys. J. **C6**, 67 (1999)
20. ZEUS Collaboration, J. Breitweg et al.: Eur. Phys. J. **C8**, 367 (1999)
21. M.H. Seymour: Nucl. Phys. B **421**, 545 (1994)
22. J. Cvach for the H1 Collaboration: 'Real and Virtual Photon Structure from Dijet events'. In: *Proc. 7th International Workshop on Deep-Inelastic Scattering and QCD (DIS99) Zeuthen, Germany, 1999*
23. R. Engel: Z. Phys. C **66**, 203 (1995)
24. R. Engel and J. Ranft: Phys. Rev. D **54**, 4244 (1996)
25. M. Glück, E. Reya and A. Vogt: Phys. Rev. D **46**, 1973 (1992)
26. M. Glück, E. Reya and A. Vogt: Z. Phys. C **53**, 127 (1992)

27. M. Glück, E. Reya and A. Vogt: Phys. Rev. D **45**, 3986 (1992)
28. L.E. Gordon and J.K. Storrow: Nucl. Phys. B **489**, 405 (1997)
29. P. Aurenche, J. Guillet and M. Fontannaz: Z. Phys. C **64**, 621 (1994)
30. M. Klasen, *these proceedings*
31. H1 Collaboration: 'Study of the photon remnant in resolved processes at HERA' *Contributed Paper 157j, International Europhysics Conference on High Energy Physics (HEP99), Tampere, Finland, 1999*
32. ZEUS Collaboration, J. Breitweg et al.: Phys. Lett. B **413**, 201 (1997)
33. N. Macdonald for the ZEUS Collaboration: 'Structure of Real and Virtual Photons from ZEUS'. In: *Proc. 7th International Workshop on Deep-Inelastic Scattering and QCD (DIS99) Zeuthen, Germany, 1999*
34. G. Schuler and T. Sjöstrand: Phys. Lett. B **376**, 193 (1996)
35. G. Ingelman, A. Edin and J. Rathsman, Comp. Phys. Commun. **101**, 108 (1997)
36. ZEUS Collaboration: 'High-Mass Dijet Cross Sections in Photoproduction at HERA' *Contributed Paper 805, International Conference on High Energy Physics (ICHEP98), Vancouver, Canada, 1998*
37. ZEUS Collaboration, J. Breitweg et al.: Phys. Lett. B **443**, 394 (1998)
38. S. Catani, Yu.L. Dokshitzer, M.H. Seymour and B.R. Webber: Nucl. Phys. B **406**, 187 (1993)
39. S.D. Ellis and D.E. Soper: Phys. Rev. D **48**, 3160 (1993)
40. ZEUS Collaboration: 'Measurements of Jet Substructure in Photoproduction at HERA' *Contributed Paper 530, International Europhysics Conference on High Energy Physics (HEP99), Tampere, Finland, 1999*